HITACHI

GE Hitachi Nuclear Energy

James F. Harrison

GE-Hitachi Nuclear Energy Americas LLC
Vice President, Fuel Licensing, Regulatory Affairs
P.O. Box 780, M/C A-55
Wilmington, NC 28401 USA

T 910.819.6604
james.harrison@ge.com

Proprietary Notice
This letter transmits proprietary information in accordance with 10 CFR 2.390. Upon the removal of Enclosure 1, the balance of the letter may be considered non-proprietary.

MFN 10-355
December 17, 2010

U.S. Nuclear Regulatory Commission
Document Control Desk
Washington, D.C. 20555-0001

Subject: Response to Request for Additional Information Re: GE-Hitachi Nuclear Energy Americas Topical Report NEDC-33173P, Revision 2 and Supplement 2, Parts 1-3 - Analysis of Gamma Scan Data and Removal of Safety Limit Critical Power Ratio Margin (TAC No. ME1891)

By Reference 1, the NRC requested additional information to support its review of NEDC-33173P, Revision 2 and Supplement 2, Parts 1-3 - Analysis of Gamma Scan Data and Removal of Safety Limit Critical Power Ratio Margin. Enclosed are responses to all of the Reference 1 RAIs.

Please note that Enclosure 1 contains proprietary information of the type that GEH maintains in confidence and withholds from public disclosure. The information has been handled and classified as proprietary to GEH as indicated in its affidavit. The affidavit contained in Enclosure 2 identifies that the information contained in Enclosure 1 has been handled and classified as proprietary to GEH. GEH hereby requests that the information in Enclosure 1 be withheld from public disclosure in accordance with the provisions of 10 CFR 2.390 and 9.17.

If you have any questions, please contact Brian Moore at (910) 819-6684 or me.

Sincerely,

James F Harrison

James F. Harrison
Vice President, Fuel Licensing
Regulatory Affairs
GE Hitachi Nuclear Energy

D065
NRO

Project No. 710

References:

1. Letter from S. S. Philpott (US NRC) to J. G. Head (GE Hitachi), Subject: Request for Additional Information Re: GE-Hitachi Nuclear Energy Americas Topical Report NEDC-33173P, Revision 2 and Supplement 2, Parts 1-3 - Analysis of Gamma Scan Data and Removal of Safety Limit Critical Power Ratio Margin (TAC No. ME1891), October 27, 2010, MFN 10-349.

Enclosures:

1. Response to NRC RAIs - NEDC-33173P, Revision 2 and Supplement 2, Parts 1-3 – GEH Proprietary Information
2. Response to NRC RAIs - NEDC-33173P, Revision 2 and Supplement 2, Parts 1-3 – Non-Proprietary Information
3. Affidavit

cc: SS Philpott, NRC
JG Head, GEH Wilmington
PL Campbell, GEH Washington
AA Lingenfelter, GNF Wilmington
eDRF Section 0000-0078-7546-R3

ENCLOSURE 1

MFN 10-355

Response to NRC RAIs - NEDC-33173P, Revision 2 and Supplement 2, Parts 1-3

GEH Proprietary Information – Class III (Confidential)

PROPRIETARY INFORMATION NOTICE

This enclosure contains proprietary information of the GE-Hitachi Nuclear Energy (GEH) and is furnished in confidence solely for the purpose(s) stated in the transmittal letter. No other use, direct or indirect, of the document or the information it contains is authorized. Furnishing this enclosure does not convey any license, express or implied, to use any patented invention or, except as specified above, any proprietary information of GEH disclosed herein or any right to publish or make copies of the enclosure without prior written permission of GEH.

The header of each page in this enclosure carries the notation "GEH Proprietary Information." GEH proprietary information is identified by a dotted underline inside double square brackets. [[This sentence is an example.{3}]]. In each case, the superscript notation{3} refers to Paragraph (3) of the enclosed affidavit, which provides the basis for the proprietary determination. Specific information that is not so marked is not GEH proprietary.

Regarding Appendix B of Enclosure 1, the header of each page in this enclosure carries the notation "GEH Proprietary Information{3} – Class III (Confidential)." The superscript notation {3} refers to Paragraph (3) of the enclosed affidavit, which provides the basis for the proprietary determination. Appendix B is an archive document not prepared for submittal to the US NRC. It is deemed GEH Proprietary in its entirety.

ENCLOSURE 2

MFN 10-355

Response to NRC RAIs - NEDC-33173P, Revision 2 and Supplement 2, Parts 1-3

Non-Proprietary Information – Class I (Public)

INFORMATION NOTICE

This is a non-proprietary version of Enclosure 1 to MFN 10-355, from which the proprietary information has been removed. Portions of the enclosure that have been removed are indicated by an open and closed bracket as shown here [[ ]]

ENCLOSURE 3

MFN 10-355

Affidavit

GE-Hitachi Nuclear Energy Americas LLC

AFFIDAVIT

I, James F. Harrison, state as follows:

(1) I am Vice President, Fuel Licensing, Regulatory Affairs, GE-Hitachi Nuclear Energy Americas LLC ("GEH"), and have been delegated the function of reviewing the information described in paragraph (2) which is sought to be withheld, and have been authorized to apply for its withholding.

(2) The information sought to be withheld is contained in Enclosure 1 of GEH letter, MFN 10-355, J. F. Harrison (GEH) to Document Control Desk (USNRC), Subject: *Response to Request for Additional Information Re: GE-Hitachi Nuclear Energy Americas Topical Report NEDC-33173P, Revision 2 and Supplement 2, Parts 1-3 - Analysis of Gamma Scan Data and Removal of Safety Limit Critical Power Ratio Margin (TAC No. ME1891)*, dated December 17, 2010. With the exception of Appendix B, the proprietary information in Enclosure 1, "Response to NRC RAIs - NEDC-33173P, Revision 2 and Supplement 2, Parts 1-3," is identified by a single dotted underline within double square brackets. [[This sentence is an example.{3}]] Regarding Appendix B of Enclosure 1, the header of each page in this enclosure carries the notation "GEH Proprietary Information{3} – Class III (Confidential)." Appendix B is deemed GEH Proprietary in its entirety. In all cases, the superscript notation {3} or {3} refers to Paragraph (3) of the enclosed affidavit, which provides the basis for the proprietary determination.

(3) In making this application for withholding of proprietary information of which it is the owner or licensee, GEH relies upon the exemption from disclosure set forth in the Freedom of Information Act ("FOIA"), 5 USC Sec. 552(b)(4), and the Trade Secrets Act, 18 USC Sec. 1905, and NRC regulations 10 CFR 9.17(a)(4), and 2.390(a)(4) for "trade secrets" (Exemption 4). The material for which exemption from disclosure is here sought also qualify under the narrower definition of "trade secret", within the meanings assigned to those terms for purposes of FOIA Exemption 4 in, respectively, Critical Mass Energy Project v. Nuclear Regulatory Commission, 975F2d871 (DC Cir. 1992), and Public Citizen Health Research Group v. FDA, 704F2d1280 (DC Cir. 1983).

(4) Some examples of categories of information which fit into the definition of proprietary information are:

a. Information that discloses a process, method, or apparatus, including supporting data and analyses, where prevention of its use by GEH's competitors without license from GEH constitutes a competitive economic advantage over other companies;

b. Information which, if used by a competitor, would reduce his expenditure of resources or improve his competitive position in the design, manufacture, shipment, installation, assurance of quality, or licensing of a similar product;

c. Information which reveals aspects of past, present, or future GEH customer-funded development plans and programs, resulting in potential products to GEH;

d. Information which discloses patentable subject matter for which it may be desirable to obtain patent protection.

The information sought to be withheld is considered to be proprietary for the reasons set forth in paragraphs (4)a. and (4)b. above.

(5) To address 10 CFR 2.390(b)(4), the information sought to be withheld is being submitted to NRC in confidence. The information is of a sort customarily held in confidence by GEH, and is in fact so held. The information sought to be withheld has, to the best of my knowledge and belief, consistently been held in confidence by GEH, no public disclosure has been made, and it is not available in public sources. All disclosures to third parties, including any required transmittals to NRC, have been made, or must be made, pursuant to regulatory provisions or proprietary agreements which provide for maintenance of the information in confidence. Its initial designation as proprietary information, and the subsequent steps taken to prevent its unauthorized disclosure, are as set forth in paragraphs (6) and (7) following.

(6) Initial approval of proprietary treatment of a document is made by the manager of the originating component, the person most likely to be acquainted with the value and sensitivity of the information in relation to industry knowledge, or subject to the terms under which it was licensed to GEH. Access to such documents within GEH is limited on a "need to know" basis.

(7) The procedure for approval of external release of such a document typically requires review by the staff manager, project manager, principal scientist, or other equivalent authority for technical content, competitive effect, and determination of the accuracy of the proprietary designation. Disclosures outside GEH are limited to regulatory bodies, customers, and potential customers, and their agents, suppliers, and licensees, and others with a legitimate need for the information, and then only in accordance with appropriate regulatory provisions or proprietary agreements.

(8) The information identified in paragraph (2) above is classified as proprietary because it contains results and details of power distribution validation data for an operating boiling water reactor using Gamma Scan measurements. Development of these methods, techniques, and information and their application for the design, modification, and analyses methodologies and processes for power distribution validation was achieved at a significant cost to GEH.

The development of the evaluation process along with the interpretation and application of the analytical results is derived from the extensive experience database that constitutes a major GEH asset.

(9) Public disclosure of the information sought to be withheld is likely to cause substantial harm to GEH's competitive position and foreclose or reduce the availability of profit-making opportunities. The information is part of GEH's comprehensive BWR safety and technology base, and its commercial value extends beyond the original development cost. The value of the technology base goes beyond the extensive physical database and analytical methodology and includes development of the expertise to determine and apply the appropriate evaluation process. In addition, the technology base includes the value derived from providing analyses done with NRC-approved methods.

The research, development, engineering, analytical and NRC review costs comprise a substantial investment of time and money by GEH.

The precise value of the expertise to devise an evaluation process and apply the correct analytical methodology is difficult to quantify, but it clearly is substantial.

GEH's competitive advantage will be lost if its competitors are able to use the results of the GEH experience to normalize or verify their own process or if they are able to claim an equivalent understanding by demonstrating that they can arrive at the same or similar conclusions.

The value of this information to GEH would be lost if the information were disclosed to the public. Making such information available to competitors without their having been required to undertake a similar expenditure of resources would unfairly provide competitors with a windfall, and deprive GEH of the opportunity to exercise its competitive advantage to seek an adequate return on its large investment in developing and obtaining these very valuable analytical tools.

I declare under penalty of perjury that the foregoing affidavit and the matters stated therein are true and correct to the best of my knowledge, information, and belief.

Executed on this 17th day of December 2010.

James F. Harrison

James F. Harrison
Vice President, Fuel Licensing,
Regulatory Affairs
GE-Hitachi Nuclear Energy Americas LLC

ENCLOSURE 2

MFN 10-355

Response to NRC RAIs - NEDC-33173P, Revision 2
and Supplement 2, Parts 1-3

Non-Proprietary Information – Class I (Public)

INFORMATION NOTICE

This is a non-proprietary version of Enclosure 1 to MFN 10-355, from which the proprietary information has been removed. Portions of the enclosure that have been removed are indicated by an open and closed bracket as shown here. [[ ]]

RAI 1

For the maps providing the locations of the scanned bundles in NEDC-33173P Supplement 2, Part 1, "Applicability of GE Methods to Expanded Operating Domains – Power Distribution Validation for Cofrentes Cycle 13," (hereafter referred to as Supplement 2 Part 1) and NEDC-33173P Supplement 2, Part 3, "Applicability of GE Methods to Expanded Operating Domains – Power Distribution Validation for Cofrentes Cycle 15," (hereafter referred to as Supplement 2 Part 3), please provide the location of the traversing in-core probe (TIP) strings.

Response

Figures 1-1 and 1-2 provide the locations of the TIP strings, with each TIP instrument tube identified by the TIP string number. The TIP string is located at the bottom, right hand corner of the bundle with the TIP string number. Note that the four bundle cells highlighted are the four bundle cells surrounding the TIP string, and do not identify the four bundles around a control rod. The TIP locations do not change between cycles; the locations of the bundles scanned in Cycles 13 and 15 are identified by the same coloring scheme used in Supplement 2 Part 1 and Supplement 2 Part 3.

[[

]]

Figure 1-1 TIP Locations in Cycle 13

[[

]]

Figure 1-2 TIP Locations in Cycle 15

RAI 2

Supplement 2 Part 1 and Supplement 2 Part 3 do not consider all of the bundle scan data in the determination of the [[ ]] *uncertainty. For the individual bundles surrounding a TIP cell that do not have three neighboring bundles (for example bundle AA0104 from Supplement 2 Part 1) is it possible to calculate the* [[ ]] *is known from the integrated TIP measurement? Please explain.*

Response

Note that bundle AA0104 is not adjacent to a TIP string in Cycle 13, and is on the periphery in another un-monitored location in Cycle 15. However, there are other TIP string locations where all four of the adjacent fuel assemblies do not have gamma scan measurements. To calculate the [[ ]] values for these cases, analytical calculated data would need to be substituted for the missing data. This process might result in improved statistics, but these statistics would be misleading and tainted by the use of analytical data. The [[ ]]. The agreement on [[ ]] such as AA0104 is considered, for example, in the overall bundle RMS statistics provided in Table 4-1 of Supplement 2 Part 1.

RAI 3

To assist the staff in comparing Cofrentes to the expanded extended power uprate (EPU) database, please provide one or two plots similar to Figure 25-19 from the Response: to RAI 25 in GE Letter (MFN 05-029), from Quintana, L., to USNRC, "Response:s to RAIs – Methods Interim Process (TAC No. MC5780)," dated April 8, 2005 characterizing the trends in TIP error with [[ ]]; please compare the Cofrentes cycle 13 and 15 data to the expanded database.

Response

The requested information is provided in Figure 3-1. As can be seen, the Cofrentes Cycle 13 and 15 data are quite compatible with the information in Figure 25-19 from the response to RAI 25 in MFN 05-029. In each case, no dependency of the [[

]] relationship with approximately the same slope for each curve as compared to Figure 25-19.

[[

]]

Figure 3-1 – TIP RMS vs. [[ ]], Cofrentes Cycles 13 and 15

RAI 4

Supplement 2 Part 3, Appendix A appears to contain several errors.

(a) The TIP comparison figures in this Appendix are labeled "Cycle 19," please reconcile this inconsistency.

(b) The units specified in the label for Figure A.2-20 are in error, please correct.

Response

All of the plots in Appendix A are corrected with "Cycle 15" rather than "Cycle 19". As an example, the corrected page A-13 is provided on the following page. The units on Figure A.2-20 have been corrected. These revisions will be included in the acceptance version of Supplement 2 Part 3.

Example of corrected page A-13:

[[

]]

RAI 5

In Figures 2.3-1 and 2.4-1 of NEDC-33173P Supplement 2, Part 2, "Applicability of GE Methods to Expanded Operating Domains – Pin-by-Pin Gamma Scan at FitzPatrick October 2006," (hereafter referred to as Supplement 2 Part 2) please indicate where the nearest instrument tube is located relative to the scanned bundles.

Response

Figure 5-1 provides the locations of the TIP strings in FitzPatrick, with each TIP instrument tube identified by the TIP string number. The TIP string is located at the bottom, right hand corner of the bundle with the TIP string number. Note that the four bundle cells highlighted are the four bundle cells surrounding the TIP string, and do not identify the four bundles around a control rod. Note that JLD505 is not adjacent to an instrument tube in either Cycle 16 or 17, while JLM420 is adjacent to an instrument tube in Cycle 17.

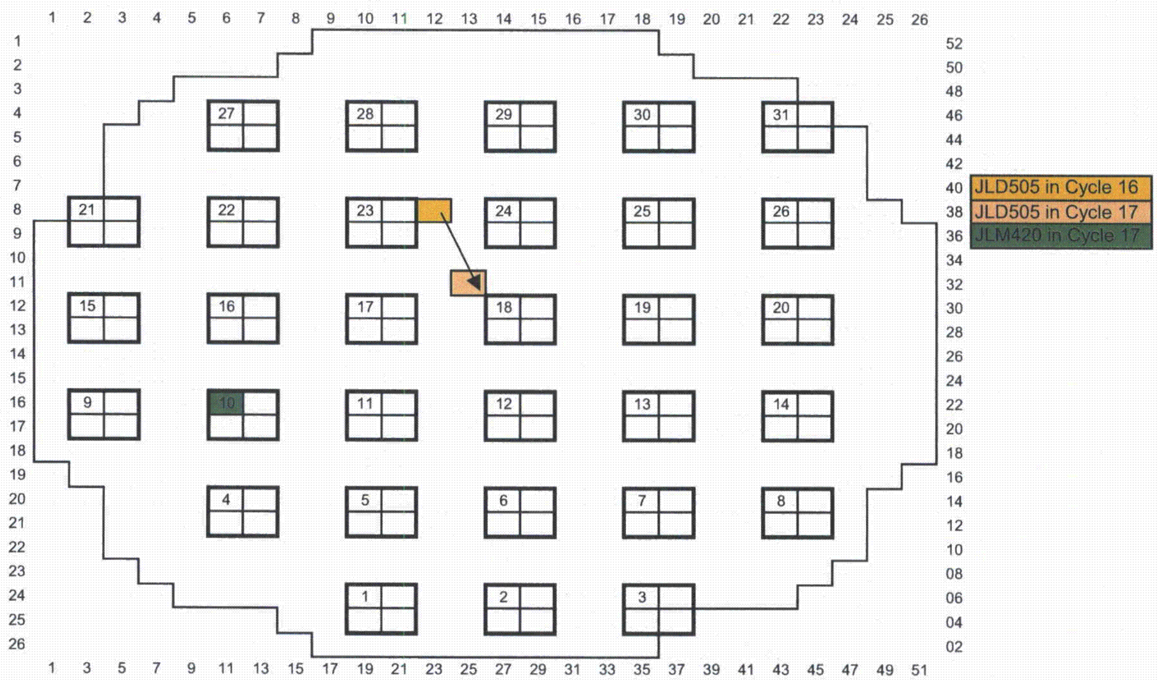

Figure 5-1 – TIP Locations for FitzPatrick

RAI 6

Please provide a figure that depicts the axial elevations where scans were performed relative to the axial geometric features of the GE14 bundles. This figure should illustrate the location of spacers and part length rods.

Response

Figure 6-1 provides the requested visualization (the top peaked axial power shape at EOC is also provided). The two measured bundles are standard GE14 designs, each having the same axial heights of the spacers, full, and part length rods. Spacers are indicated by red squares; measurement points by red triangles. The part length rod heights are also visualized.

[[

]]

Figure 6-1 Visualization of Axial Heights

RAI 7

In Section 2.7 of Supplement 2 Part 2, should "Cycle 7" read "Cycle 17"?

Response

That is correct. The acceptance version of Supplement 2 Part 2 will include this correction. (See Appendix A)

RAI 8

Please provide a series of figures that are substantially similar to Figures 2.7-1 through 2.7-4 except please plot the key operating parameters for bundle JLD505 during cycle 16.

Response

Figures 8-1, 8-2, 8-3, and 8-4 provide the requested information.

[[

]]

Figure 8-1 Maximum Bundle Power in MWt vs. Cycle 16 Exposure

[[

]]

Figure 8-2 Maximum Power / Flow Ratio vs. Cycle 16 Exposure

[[

]]

Figure 8-3 Exit Void Fraction vs. Cycle 16 Exposure

[[

]]

Figure 8-4 Peak LHGR vs. Cycle 16 Exposure

RAI 9

Please clarify how the statistics are determined for regions of the bundle where there are empty and vanished pin locations. That is, in Section 6.1, please provide a better description of how J is used if J is axially dependent.

Response

With axially varying numbers of fuel rods (empty and vanished pin locations), it is again useful to first clarify the normalization process used in comparing measured and calculated values. For multiple measurements on the same rod, an average (nodal) value is first calculated for each of the measurement points.

Thus, some rods may have more measurements than other rods; however, for the comparison process, each (nodal) measurement uses one (average) value for that location. These measurement values are relative values; the measurement data and the calculated data is first normalized so that the average value is 1.000 over all measured nodes.

Note that Section 6 has been revised to provide additional details on the process used to produce the statistics provided in Section 6. As a complicating factor, the TGBLA based process only uses node centered measurements, consistent with the nodalization used in the PANAC11 3D process.

Table 9-1 compares the number or pin measurements for the two bundles at each axial height, while Table 9-2 provides this same information for the PANAC11 based statistics.

Table 9-1 Number of Measurements Used in TGBLA Statistical Comparisons

Height from BAZ, in.	JLD505	JLM420
27	42	58
45	54	58
63	54	58
81	54	58
87	46	49
93	46	49
99	46	49
111	46	49
123	46	49
Total	434	477

BAZ: Bottom of the Active (Fuel) Zone

Table 9-2 Number of Measurements Used in PANAC11 Statistical Comparisons

Height from BAZ, in.	JLD505	JLM420
27	42	58
45	54	58
63	54	58
81	54	58
87	46	49
90	46	49
93	46	49
99	46	49
102	46	49
111	46	49
123	46	49
Total	526	575

BAZ: Bottom of the Active (Fuel) Zone

For the pin nodal RMS calculation, the normalized measured data is directly compared to the normalized calculated data as described in Section 6.1.2. Note that this equation has been revised for clarity, incorporating N = Total number of measurements. Also note that these comparisons for pin nodal RMS are not intended to depict a precisely volumetric consistent evaluation of relative nodal powers as would be obtained from a full three-dimensional evaluation with PANAC11. As is clear from the response to RAI 6, the measurement points are not equally spaced and do not represent the same volumetric sizes. Rather, the available measurement values are compared to the corresponding predicted values.

For the rod RMS calculation, this same data set is used to calculate the average value for each rod. Different rods will have different numbers of data points, with more data points for full length rods than for part length rods. In addition, some data points for some rods may be missing because of measurement difficulties. For each of the fuel rods, the average value of the measured data for that rod is then compared to the predicted values, where the number of data points for each rod in the predicted data is exactly consistent with the number of measured data points for that rod. Thus, the average values for each fuel rod necessarily do not depict the same volumetric value. Section 6.1.3 has also been revised for clarity and will be included in the acceptance version of Supplement . (See Appendix A)

For the axial average RMS calculations, for each axial level, the averages are calculated, and the [[ ]] for each axial level is formed. The sum of these numbers is then divided by the number of axial levels. Again, Section 6.1.4 has been revised to clarify the calculation process. (See Appendix A)

For bundle JLD505, for example, the number of axial levels measured for full length rods is [[ ]]. To further clarify this calculation see Table 9-3 for bundle JLD505. Again, the number of rod measurements used at each axial level is not the same, due to (a) part length rods and (b) experimental difficulties in the first axial height.

Table 9-3 Details Axial Average RMS for Bundle JLD505 (Adapted Off-Line)

Height from BAZ	Avg Predicted Ba-140	Avg Measured La-140	(Avg Pred - Avg Meas)^2	Count Pred	Count Meas
[[					
					]]

RAI 10

Please clarify what is meant by "Axial Averaged RMS for Bundle..." in Section 6.5. These figures appear to depict the measured and calculated axial power distributions that are radially averaged. Please describe the differences between the figures in Section 6.5 and Figure 2.9.2.

Response

Figure 2.9-2 provides the nodal power for bundles JLM420 and JLD505 at EOC17 from the off-line unadapted PANAC11 core tracking for FitzPatrick. As such, the average nodal power for all bundles in the core is 1.00. The data presented here is for all [[ ]] nodes. Also note that Figure 2.9-2 contains no "measured" data, only calculated data. The axial power data in Figure 2.9-2 shows a reduction in the nodal power for these bundles just above the axial point where the part length rods terminate.

Using the PANAC11 core power distributions, the calculated TIPs from PANAC11 can be compared to the measured TIPs, as shown in Figure A.2-15 at EOC17 (note that this is for the core average information). The individual TIPs shown in Figure A.2-16 represent (more or less) the average of the four bundles surrounding the TIP instrument. This process of TIP comparisons is one method of validating the power distribution calculations of PANAC11. As shown in Table A.1-1, the nodal RMS for this EOC17 TIP comparison is [[ ]] The complete core is composed of GE10x10 fuel, and the EOC TIP measurements show no discernable trend at the axial point were the part length rods terminate.

The data in Section 6.5 provide a comparison of the axial averaged predicted ^{140}Ba and the measured ^{140}La of only those rods that were measured during the gamma scan campaign. Note that the "RMS" label on these plots was replaced with "Predicted Ba and Measured La". While this is only for a limited number of axial measurement points, and for only a sub-set of all the fuel rods in the fuel assembly, the comparison nevertheless provides useful insight into the capabilities for the TGBLA06 / PANAC11 system of codes to calculate the pin-by-pin power distributions within the bundles in the core, since power and ^{140}Ba are approximately linearly dependent. Both the predicted ^{140}Ba and the measured ^{140}La demonstrate an increase at the axial point were the part length rods terminate. When the data for individual rods are examined, it is seen that fuel rods on the corners of the bundle do not demonstrate nearly the magnitude of increase as those fuel rods that are more interior to the fuel assembly. That is, the specific operating conditions of individual rods produce some variances in the ^{140}Ba production rate, and the ^{140}Ba is both calculated and measured to increase above this axial point. The axial RMS for these comparisons is slightly better than the TIP nodal RMS; this is because a smaller axial range is compared, and then only for a smaller subset of fuel rods.

The robustness and detail of the TGBLA06 / PANAC11 system of codes are confirmed by this ability to correctly calculate different distributions of power, TIPs, and ^{140}Ba production.

RAI 11

To assist the staff in comparing Supplement 2 Part 2 to the traditional gamma scan qualification, please provide the following reference:

L. M. Shiraishi, Gamma Scan Measurements of the Lead Test Assembly at The Duane Arnold Energy Center Following Cycle 8, NEDC-31569-P, April 1988.

Response

This report is considered proprietary in its entirety. It is included as Appendix B to Enclosure 1.

RAI 12

Please clarify Table 7.2-1. In particular, are the standard deviations quoted in this table consistent with the traditional basis for the pin power peaking uncertainty? In other words, are these averaged root-mean-squared (RMS) differences for the different axial levels?

Response

The data in Table 7.2-1 is taken from Tables 5.2-1, 5.2-2, and 5.2-3 for bundle JLM420, and from Tables 5.3-1, 5.3-2 and 5.3-3 for bundle JLD505. The data is therefore consistent with the traditional basis for the pin power peaking uncertainty, calculated from the average standard deviation for the different axial levels.

RAI 13

Please supplement Supplement 2 Part 2 with a section that is substantially similar to Section 8.3 except based on the JLD505 gamma scan data.

Response

Section 8.3 provides 3D plots comparing [(P11/Meas) – 1] for bundle JLM420 at different elevations. Section 8.2 provides similar plots for [(TGBLA/Meas) – 1] for bundle JLM420. In a similar fashion, the comparisons for [(TGBLA/Meas) – 1] for bundle JLD505 are first provided, and then those comparing [(P11/Meas) – 1] for bundle JLD505. Note that fuel rod [[ ]] at elevation [[ ]] inches appears anomalous; while no reason has been found to exclude this one experimental point, the measurement appears suspect.

Sections 8.4 and 8.5 have been added to the Supplement 2 Part 2 report and will be included in the acceptance version. (See Appendix A) The Revision 0 Section 8.4 becomes Section 8.6.

Bundle JLD505 [(TGBLA/Meas) – 1] (Figures 13-1 to 13- 9)

[[

]]

Figure 13-1 Bundle JLD505 [(TGBLA/Meas) – 1] at 27 Inches

[[

]]

Figure 13-2 Bundle JLD505 [(TGBLA/Meas) – 1] at 45 Inches

[[

]]

Figure 13-3 Bundle JLD505 [(TGBLA/Meas) – 1] at 63 Inches

[[

]]

Figure 13-4 Bundle JLD505 [(TGBLA/Meas) – 1] at 81 Inches

[[

]]

Figure 13-5 Bundle JLD505 [(TGBLA/Meas) – 1] at 87 Inches

[[

]]

Figure 13-6 Bundle JLD505 [(TGBLA/Meas) – 1] at 93 Inches

[[

]]

Figure 13-7 Bundle JLD505 [(TGBLA/Meas) – 1] at 99 Inches

[[

]]

Figure 13-8 Bundle JLD505 [(TGBLA/Meas) – 1] at 111 Inches

[[

]]

Figure 13-9 Bundle JLD505 [(TGBLA/Meas) – 1] at 123 Inches

Bundle JLD505 [(P11/Meas) – 1] (Figures 13-10 to 13-19)

[[

]]

Figure 13-10 Bundle JLD505 [(P11/Meas) – 1] at 27 Inches

[[

]]

Figure 13-11 Bundle JLD505 [(P11/Meas) – 1] at 45 Inches

[[

]]

Figure 13-12 Bundle JLD505 [(P11/Meas) – 1] at 63 Inches

[[

]]

Figure 13-13 Bundle JLD505 [(P11/Meas) – 1] at 81 Inches

[[

]]

Figure 13-14 Bundle JLD505 [(P11/Meas) – 1] at 87 Inches

[[

]]

Figure 13-15 Bundle JLD505 [(P11/Meas) – 1] at 90 Inches

[[

]]

Figure 13-16 Bundle JLD505 [(P11/Meas) – 1] at 93 Inches

[[

]]

Figure 13-17 Bundle JLD505 [(P11/Meas) – 1] at 99 Inches

[[

]]

Figure 13-18 Bundle JLD505 [(P11/Meas) – 1] at 102 Inches

[[

]]

Figure 13-19 Bundle JLD505 [(P11/Meas) – 1] at 111 Inches

[[

]]

Figure 13-20 Bundle JLD505 [(P11/Meas) – 1] at 123 Inches

RAI 14

The [[ ]] *to be biased. However, this is based on a limited data sample. Please perform transport calculations to assess if the magnitude of the observed trend in* [[ ]]. *If the* [[ ]] *please explain the observed trend in* [[ ]].

Response

The [[ ]] to be biased, [[ ]] More detailed calculations of the [[ ]].

RAI 15

Please update Section 8.4.1 of Supplement 2 Part 2 to include a disposition of the NN rod power for plants with thermal TIPs.

Response

The impact of a difference between the design predicted and actual power of the NN rod on the TIP signal was evaluated in a conservative manner by using infinite lattice calculations. In these calculations, the NN rod power was changed by means of variation of the NN pin enrichment. The value of the flux at the detector location was obtained for each of these variations. To ascertain the impact on the TIP signal of these pin power changes, the thermal group flux changes were used. In addition, these calculations were completed at different void fractions and uncontrolled depletions over the life of the fuel assembly were evaluated.

[[

]].

Also note that if the NN rod had a higher pin power than predicted, the depletion process in the reactor would tend to "burn" this difference away; the NN rod would deplete faster and approach the nominal predicted power later in exposure. In a similar manner, if the NN rod had a lower pin power than predicted at lower exposures, it would deplete at a slower rate, and would approach the nominal predicted power later in exposure. Thus, the normal depletion process tends to self-heal biases in predicted pin powers.

Figure 15-1 provides insights as to the impact of changes in NN rod powers on the fluxes in the detector location for [[ ]]. Figure 15-2 provides insights as to the self healing process of the pin powers due to depletion. Figure 15-3 provides detailed information on the impact of changes in NN pin powers on thermal flux in the detector over the complete exposure range of the life of the fuel assembly (evaluated at [[ ]]

[[

]]

Figure 15-1 Detector Fluxes for Three Groups as a Function of Relative NN Rod Power

[[

]]

Figure 15-2 Relative NN Rod Power As a Function of Exposure

[[

]]

Figure 15-3 Impact of Changes in NN Pin Powers on the 1/(Thermal Flux in the Detector)

RAI 16

Please update Section 8.4.1 of Supplement 2 Part 2 with a discussion addressing nodal power uncertainty in addition to P4B uncertainty.

Response

Please refer to the response to RAI 14. The nodal power uncertainties resulting from a [[

]] are included in the overall statistical comparisons from the gamma scan results.

RAI 17

Please update Section 8.4.1 of Supplement 2 Part 2 with a discussion of the extrapolation of potential biases to MELLLA+ operating conditions."

Response

Please refer to the response to RAI 14. No additional impact for these potential biases are foreseen for MELLLA+ operating conditions.

RAI 18

The [[ ]] errors for the second to last exposure point provided in Appendix A for the TIP comparisons are very large compared to the expected differences [[ ]] expected). From visual inference, this error appears to be a result of large radial power differences observed for TIP strings 10 and 16. TIP string 10 is adjacent to JLM420. Please discuss the implications of these results.

Response

From sometime after April, 2006 until very near the end of cycle in October, 2006, there was a problem with one of the TIP machines. For the TIPs associated with this one machine, the values were not normalized to the same integral value as the TIP data from the other TIP machines. As a result, the nodal RMS difference between the measured and calculated TIPs increased dramatically for the June, 2006 TIP set. This problem was corrected by the last TIP set. However, this did not affect the 3DM / PANAC11 shape adaptive process, in that [[

]] calculated in the shape adaptive process were not affected, as the axial shape of the TIP measurements was not affected by the TIP mechanical problems, nor was the LPRM calibration process in 3DM / PANAC11. In addition, the exposure and void history accumulation in the on-line 3DM / PANAC11 is based on the [[ ]]. Thus, the only implication is that the TIP radial RMS for this one case is seen to be quite large, with no actual impact on plant monitoring due to the inherent robustness of the 3DM / PANAC11 system.

RAI 19

Please explain how the average corrected standard deviation in the tables in Section 5 of Supplement 2 Part 2 is calculated.

Response

First we define $\sigma_{experiment}$ as the standard deviation of [(Calculated / Measured) minus 1] at some given elevation, and $\sigma_{reference}$ as the standard deviation of repeat measurements of the activity of the [[ ]]. For each axial level, the "Corrected Standard Deviation" at that axial level for the "traditional" process is evaluated by calculating $\sigma_{corrected}$ as follows:

[[ ]]

After the $\sigma_{corrected}$ is calculated at each axial level, the average value for all axial nodes is then calculated.

It is recognized that this process, used for the Duane Arnold pin-by-pin gamma scan in evaluating the "1986 Lead Test Assembly" data [[ ]].

RAI 20

Table 2-11 of NEDC-33173P, "Applicability of GE Methods to Expanded Operating Domains," Revision 2, includes a correction to the update uncertainty. The staff notes that the corrected Revision 0, linear heat generation rate (LHGR) uncertainty is [[ ]]percent. The updated uncertainty is expected to be a function of the exposure interval between local power range monitor (LPRM) calibrations.

(a) *Please provide descriptive details regarding the basis for the quantification of this uncertainty component. This description should address the component of the update uncertainty attributed to instrument failure.*

(b) *Upon cursory review of NEDC-32694P-A, "Power Distribution Uncertainties for Safety Limit MCPR Evaluations," Appendix B, the basis appears to be based on[[ ]]. Please justify how these results are representative for the entire fleet.*

(c) *Upon cursory review of NEDC-32694P-A, Appendix B, it would appear that if [[ ]]. Please justify the applicability of these data to quantify an uncertainty associated with calibration intervals of [[ ]] MWD/T or higher.*

(d) *Please specify the maximum LPRM calibration interval (in terms of exposure) to which the generic NEDC-32694P-A, Appendix B, update uncertainty value is applicable.*

(e) *Please justify the LPRM calibration interval provided in (d). In this justification, please consider the standard technical specifications (STS) surveillance requirement (SR) 3.0.2 which allows a 25 percent extension of the calibration interval to address potential plant conditions impairing calibration.*

(f) *Several plants have applied for LPRM calibration interval extensions. If a plant with an extended LPRM calibration interval applies for an EPU, please describe how the plant-specific LPRM calibration interval is accounted for in the uncertainty analysis.*

(g) *Several plants that have applied for LPRM calibration interval extensions have referenced improved LPRM devices (e.g., NA300 series devices). Please describe how the plant-specific hardware is considered in the safety analyses for plants referencing the IMLTR.*

(h) *Several plants have applied for LPRM calibration interval extensions and justified the approach relative to the nodal uncertainty analysis provided under the GE Thermal Analysis Basis (NEDE-10958P-A, "General Electric Thermal Analysis Basis Data, Correlation and Design Application"). When these plants reference the IMLTR, component uncertainties are reduced, such as [[ ]] These* *reduced uncertainties are consistent with the improved 3D MONICORE system. Therefore, conservatism credited in the safety evaluation for the initial LPRM calibration interval does not exist when these plants reference the IMLTR as the basis for their safety limit uncertainties. Please explain how the extended LPRM calibration interval is considered in the safety analysis for these plants.*

(i) *Several plants define the LPRM calibration interval in units of effective full power hours (EFPH). Plants that define the interval using units of EFPH that apply for an EPU are likewise applying for an extension of the LPRM calibration interval in terms of accumulated exposure between calibrations. Please explain how these plants are addressed in the IMLTR based LHGR uncertainty analysis?*

Response

Before answering each of the specific concerns, additional information is first supplied which supplements information previously provided. LPRM update uncertainties for currently operating BWRs with modern fuel designs and current LPRM detector types have been examined for a representative population of the BWR fleet. The purpose for this new information is to demonstrate that the LPRM update uncertainty is not exposure dependent over a wide range of exposure increments between TIP / LPRM calibrations.

New Information

To evaluate the LPRM uncertainty, it is only necessary to evaluate the difference in the core peak thermal margins before and after a TIP set, which can be obtained directly from plant data. Current data was obtained from seven plants and twelve cycles of these seven plants, as shown in Table 20-1. As can be seen, this list of plants includes D, C, and S lattices, small plants and large plants, and both thermal (neutron) TIP monitoring systems and gamma (γ) TIP monitoring systems.

Table 20-1 Types of Plants Analyzed

Plant Name	BWR/ Type	Lattice Type	# of Bundles	TIP Type	Cycles
Plant "A"	[[				
Plant "B"					
Plant "C"					
Plant "D"					
Plant "E"					
Plant "F"					
Plant "G"					]]

A total of 115 TIP / LPRM calibrations were examined for the seven plants (twelve different cycles for these seven plants). For each TIP set during the cycle, the peak thermal margins determined by LPRM adaption just prior to the TIP set can be compared to the thermal margins determined by LPRM adaption for the first 3DM case following the TIP set. The three thermal margins compared are TIP and LPRM adapted thermal margins:

- MFLPD : maximum fraction of linear power density: ratio of the maximum rod linear heat generation rate (MLHGR) to the LHGR limit. This is based on the peak linear heat generation rate for any particular fuel rod.
- MAPRAT: ratio of maximum average node planar linear heat generation rate to the limit. This is a measure of the nodal power, as it is the average linear heat generation rate of all fuel pins at that axial elevation for that bundle
- MFLCPR: maximum fraction of limiting critical power ratio (proportional to the inverse bundle power).

Some of the plants analyzed have already extended the period between TIP / LPRM calibrations to [[ ]] EFPH. The data from these operating plants includes [[ ]].

The LPRM instrumentation types for these seven plants are summarized in Table 20-2. BWR/6 plants normally use NA250's. As shown in Table 2 the remainder of the plants use NA300 LPRM detectors.

Table 20-2 – Types of LPRM Detectors

Plant Name	Cycle	Number LPRMs	Number LPRM Strings	Fraction NA250	Fraction NA300	Fraction Empty
Plant "A"	[[					
Plant "B"						
Plant "B"						
Plant "C"						
Plant "D"						
Plant "D"						
Plant "E"						
Plant "E"						
Plant "F"						
Plant "F"						
Plant "G"						
Plant "G"						]]

Results

As shown in Figures 20-1, 20-2, and 20-3, the LPRM update uncertainty evaluations demonstrate essentially no exposure dependency. As summarized in Table 20-3, the one sigma (Standard Deviation or RMS) uncertainty values are well within the currently accepted GNF licensing basis for LPRM update uncertainty. In particular, the current LPRM update uncertainty of [[ ]] is quite well supported by the summary data provided in Table 20-3, "% Change in MFLPD".

Table 20-3 Summary of LPRM Update Uncertainties

	% Change in MFLCPR	% Change in MFLPD	% Change in MAPRAT
Std Dev	[[		
RMS			]]

MFLCPR COMPARISONS

Figure 20-1 summarizes the MFLCPR comparisons for the seven plants. As can be seen, the data over the full exposure range from zero exposure to [[ ]] MWd/ST show no dependency with the exposure interval between the TIP / LPRM calibrations.

[[

]]

Figure 20-1 MFLCPR LPRM Update- Change in Thermal Margin Following LPRM Calibration

MFLPD COMPARISONS

Figure 20-2 summarizes the MFLPD comparisons for the seven plants. As can be seen, the data over the full exposure range from zero exposure to [[ ]] MWd/ST show a very slight upward rise as a function of the exposure interval between the TIP / LPRM calibrations.

[[

]]

Figure 20-2 MFLPD LPRM Update- Change in Thermal Margin Following LPRM Calibration

MAPRAT COMPARISONS

Figure 20-3 summarizes the MAPRAT comparisons for the seven plants. As can be seen, the data over the full exposure range from zero exposure to [[ ]] MWd/ST show a slight upward rise as a function of the exposure interval between the TIP / LPRM calibrations.

[[

]]

Figure 20-3 MAPRAT LPRM Update- Change in Thermal Margin Following LPRM Calibration

Specific Responses

RAI 20 (a)

(a) *Please provide descriptive details regarding the basis for the quantification of this uncertainty component. This description should address the component of the update uncertainty attributed to instrument failure.*

Response

The pertinent portion of Table 2-11 is provided below:

Table 2-11 Summary of Uncertainty Components for LHGR Evaluations

Component	NEDE-32601 (1)	Revision 0 (1)	Revision 0 (2)	Revision 2
[[				]]

Notes from NEDC-33173P Rev 2:

(1) Values from NEDC-33173P Revision 0 Safety Evaluation Table 3-11 [Reference 37]

(2) Separate from the Methods LTR Supplement 2 uncertainty qualification, it was noticed that the update uncertainty should be [[ ]] as stipulated in RAI II.5 of NEDC-32694P-A [Reference 13].

As can be seen, there was no specification of the contributions to LHGR impacts due to failed TIP and LPRMs.

As shown in Table 20-3 above, a value of [[ ]] for the LPRM update uncertainty has been derived from plant data. This plant data (115 points) represents 7 plants, 12 cycles, both gamma and neutron TIPs, and includes conditions with failed LPRMs and failed TIPs. The resulting [[ ]] uncertainty can clearly be applied across the data range to an exposure of approximately [[ ]] MWD/ST. The trends, as discussed in the response to RAI 20(d), suggest that the [[ ]] uncertainty is conservative to an exposure of [[ ]].

To be consistent with the above discussion, the line denoting Update uncertainty in Table 2-11 will be modified in the acceptance version of NEDC-33173P to include the revised component definition and the additional note.

Revised Table 2-11 Summary of Uncertainty Components for LHGR Evaluations

Component	NEDE-32601 (1)	Revision 0 (1)	Revision 0 (2)	Revision 2
[[				]]

(1) Values from NEDC-33173P Revision 0 Safety Evaluation Table 3-11 [Reference 37]

(2) Separate from the Methods LTR Supplement 2 uncertainty qualification, it was noticed that the update uncertainty should be [[ ]] as stipulated in RAI II.5 of NEDC-32694P-A [Reference 13].

(3) This component of the LHGR uncertainty is valid up to an exposure of [[ ]] MWD/ST.

RAI 20 (b)

(b) *Upon cursory review of NEDC-32694P-A Appendix B, the basis appears to be based on* [[ ]], *during which* [[ ]] *TIP measurements were made. Please justify how these results are representative for the entire fleet.*

Response

The re-evaluation of this item is now based on a much larger set of data representative of the entire fleet.

RAI 20 (c)

(c) *Upon cursory review of NEDC-32694P-A Appendix B, it would appear that if* [[ ]] *TIP measurements were considered for* [[ ]] *that the exposure interval between the LPRM calibrations would be less than* [[ ]] *MWD/T. If a cycle exposure of* [[ ]] *GWD/T is assumed, the interval between LPRM calibrations, on average, would only be* [[ ]]*MWD/T. Please justify the applicability of these data to quantify an uncertainty associated with calibration intervals of* [[ ]] *MWD/T or higher.*

Response

Based on the new data documented previously and illustrated in Figures 20-1, 20-2, and 20-3 above, there is essentially no exposure dependency to the LPRM update uncertainty for any of the thermal margins. The trend, as a function of exposure increment between TIP sets, demonstrates that the LPRM depletion models are functioning as designed within the calibration interval and that there are no non-linear affects. The plant data [[ ]] represents 7 plants, 12 cycles, both gamma and neutron TIPs, and includes conditions with failed LPRMs and failed TIPs. The resulting [[ ]] uncertainty can be applied to an exposure of approximately [[ ]] MWD/ST. Therefore, the [[ ]] uncertainty as currently specified is conservative.

RAI 20 (d)

(d) *Please specify the maximum LPRM calibration interval (in terms of exposure) to which the generic NEDC-32694P-A Appendix B update uncertainty value is applicable.*

Response

Using the minor linear slope of the average error from the fit of the data as shown on Figure 20-2 the average error at [[ ]] is calculated to be [[ ]]. Using this value and the same standard deviation, [[ ]], the total RMS error is estimated to be [[ ]], leaving margin to the [[ ]] which is applied in the overall uncertainty evaluation for the linear heat generation rate. Therefore, the maximum calibration interval is conservatively specified to be [[ ]].

To further examine the data, consider the two outliers on Figure 20-2:

- [[ ]] is well in excess of 4σ from the standard deviation of the data, and,
- [[ ]] is roughly 3.7σ from the standard deviation of the data.

These extreme points are included in the Figure 20-2 statistics and significantly affect the appearance of a trend as well as the standard deviation. Note that these points are included in the above determination that [[ ]] is conservative to an exposure of [[ ]].

For the purpose investigation, we will eliminate the [[ ]] points, divide the data into exposure intervals, and calculate the standard deviation for the different exposure intervals. The data points were separated into three different exposure ranges of equal exposure ([[ ]]). Figure 20-4 demonstrates that for the three exposure groups there is very little variation in the standard deviation of the change in the MFLPD thermal margins before and after TIP / LPRM calibrations.

[[

]]

Figure 20-4 Change in Standard Deviation with Exposure for MFLPD

RAI 20 (e)

(e) *Please justify the LPRM calibration interval provided in (d). In this justification please consider the standard technical specifications (STS) surveillance requirement (SR) 3.0.2 which allows a 25 percent extension of the calibration interval to address potential plant conditions impairing calibration.*

Response

As presented in the response to RAI 20 (d), the maximum LPRM calibration interval can be at least [[ ]] MWd/ST. Based on the 25% extension allowance a technical specifications (TS) calibration interval of [[ ]] MWd/ST is supported. For a particular plant, the specific TS extension allowance would determine the appropriate TS calibration interval.

RAI 20 (f)

(f) *Several plants have applied for LPRM calibration interval extensions. If a plant with an extended LPRM calibration interval applies for an EPU, please describe how the plant-specific LPRM calibration interval is accounted for in the uncertainty analysis.*

Response

Because no exposure dependency to the thermal margin LPRM update uncertainty was observed in Figures 20-1, 20-2, and 20-3 of this document, and since the plants included data for EPU operation, there is no need to make any special accounting in the uncertainty analyses for these plants.

RAI 20 (g)

(g) *Several plants that have applied for LPRM calibration interval extensions have referenced improved LPRM devices (e.g., NA300 series devices). Please describe how the plant-specific hardware is considered in safety analyses for plants referencing the IMLTR.*

Response

Because the data provided in this memo includes a large amount of data derived from plants with NA300 series devices, no special consideration for NA300 series devices is necessary.

RAI 20 (h)

(h) Several plants have applied for LPRM calibration interval extensions and justified the approach relative to the nodal uncertainty analysis provided under GE Thermal Analysis Basis (NEDO-10958P-A). When these plants reference the IMLTR, component uncertainties are reduced, such as the gradient uncertainty. These reduced uncertainties are consistent with the improved 3D MONICORE system. Therefore, conservatism credited in the safety evaluation for the initial LPRM calibration interval does not exist when these plants reference the IMLTR as the basis for their safety limit uncertainties. How is the extended LPRM calibration interval considered in the safety analysis for these plants?

Response

See the Response: for item (f) above.

RAI 20 (i)

(i) *Several plants define the LPRM calibration interval in units of effective full power hours (EFPH). Plants that define the interval using units of EFPH that apply for an EPU are likewise applying for an extension of the LPRM calibration interval in terms of accumulated exposure between calibrations. How are these plants addressed in the IMLTR based LHGR uncertainty analysis?*

Response

The translation between EFPH and MWd/ST exposure accumulation between calibrations depends on the rated power of the plant and the core weight of the fuel in the core for that particular cycle. The MWd/ST/Day is calculated by forming the ratio (PRATED MWt) / (Core Weight ST). The EFPH corresponding to [[ ]] MWd/ST is calculated using 24 hrs * [[ ]] MWd/ST) / (MWd/ST/Day)]. Thus for each different plant, a different EFPH corresponding to [[ ]] MWd/ST would be established. However, a more effective approach in the long term would be to use MWd/ST units in the Technical Specifications.

Appendix A – Revision 1 of NEDC-33173P Supplement 2 Part 2

As committed in the RAI responses, revisions and additional content will be incorporated into the acceptance version of Supplement 2 Part 2. In addition to the incorporation of the changes committed in the RAI responses, slight improvements in the statistical comparisons between the measured and calculated results will be incorporated. During the review as part of the RAI response process, a number of conservative inputs in various spreadsheets used to produce the statistics and plots in Supplement 2 Part 2 were identified. For internal consistency, the affected portions of the LTR have been updated and revised. The change pages follow in Appendix A. These revised pages will be the basis for the acceptance version.

The affected pages are summarized in the following table.

Page Number in Rev 1	Type of Revision	Note
2-2	Added Figure 2.1-1 showing TIP locations (added new page)	RAI 5
2-10	Added Cycle 16 information; Changed Cycle 7 to Cycle 17	RAI 7 and 8
2-11, 2-12	Added Cycle 16 information plots (new pages)	RAI 7
2-19, 2-20	Modified Figures 2.9-1, 2.9-2, and 2.9-3 to include all 11 measurement points (Verifier comment)	See EXCEL Files "Visualizing_heights.XLS" and "eoc axials.xls"
3-3	Added Figure 3.2-1 showing locations of spacers and fuel rods	RAI 5
5-3	Table 5.2-1 Revised	Spreadsheet Revision
5-4	Table 5.2-2 Revised	Spreadsheet Revision
5-7	Table 5.3-1 Revised	Spreadsheet Revision
5-8	Table 5.3-2 Revised	Spreadsheet Revision
5-12	Figure 5.4.1-2 – Replaced as Data for Elevation 111 inches is revised.	Spreadsheet Revision
5-16	Figure 5.4.1-6 – Replaced as a result.	Spreadsheet Revision
5-22 through 5-25	Figures 5.4.2-4 through 5.4.2-7 were not copied correctly from the EXCEL spreadsheet	Revision
6-1, 6-2	Equations for statistics clarified.	RAI 9
6-3	Range for pin nodal RMS for gamma scan changed from (3.9% and 5.1%) to (3.9% to 4.9%)	Spreadsheet Revision
6-4	Tables 6.2-1, 6.2-2, and 6.2-3 Revised	Spreadsheet Revision
6-5	RMS value in second paragraph and Figure 6.3.1-1 revised	Spreadsheet Revision
6-6	RMS value in second paragraph and plot revised	Spreadsheet Revision
6-8	RMS values and two figures revised	Spreadsheet Revision
6-9	RMS value and two figures revised	Spreadsheet Revision
6-10	Two figures revised for readability	Revision

Page Number in Rev 1	Type of Revision	Note
6-11	RMS value and two figures revised	Spreadsheet Revision
6-12	RMS value and two figures revised	Spreadsheet Revision
7-2	Text added to second paragraph; Table 7.2 revised	RAI 9, Spreadsheet Revision
8-2 thru 8-12	Figures 8.2-1 through 8.3-11 revised or added.	Spreadsheet Revision
8-13 thru 8-24	Sections 8.4 and 8.5 added for Bundle JLD505	RAI 13
8-25, 8-26, 8-27	Figure numbers revised.	Due to added Sections 8.4 and 8.5
8-28	New information	RAI 15
A-1	Added new third paragraph.	RAI 18

With one exception the modified statistical results show smaller values in the revised document. The only exception is seen in Table 6.2-2, page 6-4, where the revised Axial Average RMS for bundle JLD505 was revised [[ ]]

Figure 2-1 provides the locations of the TIP strings in FitzPatrick, with each TIP instrument tube identified by the TIP string number. The TIP string is located at the bottom, right hand corner of the bundle with the TIP string number. Note that the four bundle cells highlighted are the four bundle cell surrounding the TIP string, and do not identify the four bundles around a control rod. The TIP locations do not change between cycles; the locations of the bundles scanned in Cycles 16 and 17 are identified by the same coloring scheme used in Sections 2.3 and 2.4 below. Note that JLD505 is not adjacent to an instrument tube in either Cycle 16 or 17, while JLM420 is adjacent to an instrument tube in Cycle 17.

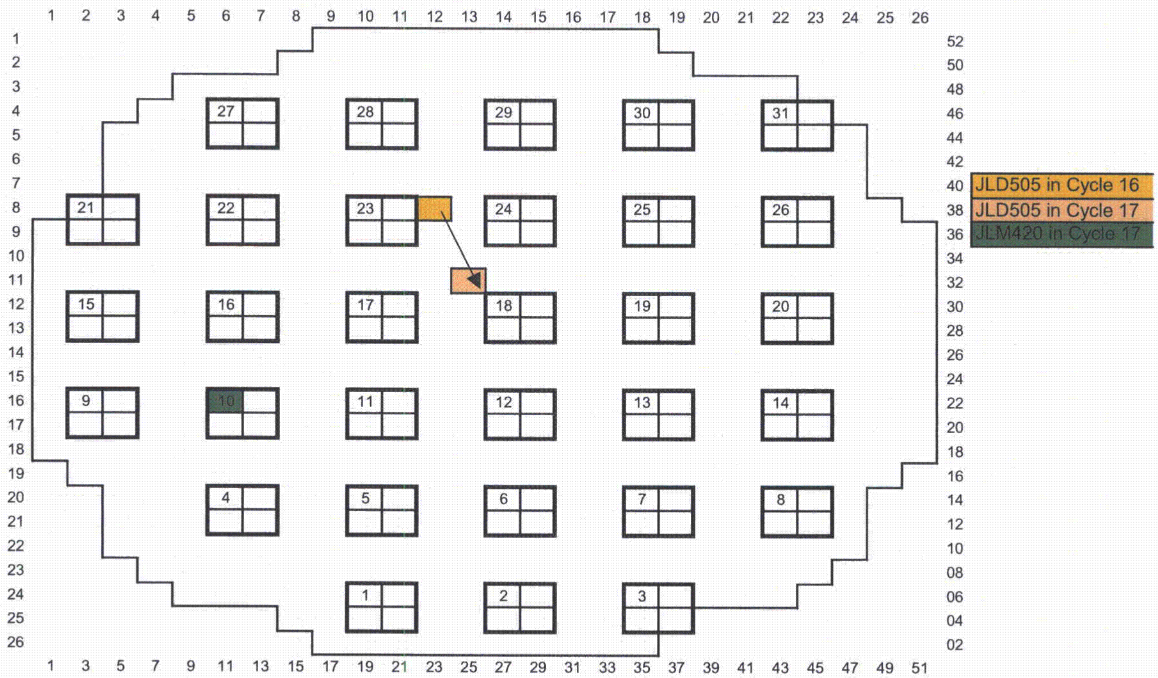

Figure 2.1-1 TIP Locations for FitzPatrick

2.7 CHARACTERIZATION OF OPERATING CONDITIONS - GAMMA SCAN BUNDLES

The purpose for this section is to characterize some of the operating parameters for the bundles used in the FitzPatrick gamma scan. The following information is based on the non-adapted off-line core tracking.

- Figure 2.7-1. provides information regarding the bundle power (expressed in MWt) as a function of Cycle 16 exposure.
- Figure 2.7-2. provides information regarding the ratio (bundle power in MWt) / (bundle flow in lb/hr) as a function of Cycle 16 exposure.
- Figure 2.7-3. provides information regarding the exit void fraction for the two gamma scan fuel assemblies as a function of Cycle 16 exposure.
- Figure 2.7-4. provides information regarding the bundle peak Linear Heat Generation Rate (LHGR) in kW/ft as a function of Cycle 16 exposure. The LHGR limit is a function of nodal exposure. The kW/ft at the node of Maximum Fraction of Limiting Power Density (MFLPD) is plotted as well as the peak kW/ft for the core and the maximum kW/ft for each of the two gamma scanned fuel bundles.
- Figure 2.7-5. provides information regarding the bundle power (expressed in MWt) as a function of Cycle 17 exposure.
- Figure 2.7-6. provides information regarding the ratio (bundle power in MWt) / (bundle flow in lb/hr) as a function of Cycle 17 exposure.
- Figure 2.7-7. provides information regarding the exit void fraction for the two gamma scan fuel assemblies as a function of Cycle 17 exposure.
- Figure 2.7-8. provides information regarding the bundle peak Linear Heat Generation Rate (LHGR) in kW/ft as a function of Cycle 17 exposure. The LHGR limit is a function of nodal exposure. The kW/ft at the node of Maximum Fraction of Limiting Power Density (MFLPD) is plotted as well as the peak kW/ft for the core and the maximum kW/ft for each of the two gamma scanned fuel bundles.

[[

]]

Figure 2.7-1. Maximum Bundle Power in MWt vs. Cycle 16 Exposure

[[

]]

Figure 2.7-2. Maximum Power / Flow Ratio vs. Cycle 16 Exposure

[[

]]

Figure 2.7-3. Exit Void Fraction vs. Cycle 16 Exposure

[[

]]

Figure 2.7-4. Peak LGHR vs. Cycle 16 Exposure

2.9 EOC17 INFORMATION

The following plots provide insights as to the nodal exposure, nodal power, and nodal void fractions seen at EOC17:

- Figure 2.9.1. EOC17 Nodal Exposures for Bundles JLM420 and JLD505
- Figure 2.9.2. EOC17 Nodal Powers for Bundles JLM420 and JLD505
- Figure 2.9.3. EOC17 Nodal Void Fractions for Bundles JLM420 and JLD505

Vertical red lines denote the axial heights at which gamma scan measurements were made.

[[

]]

Figure 2.9-1 EOC17 Nodal Exposures for Bundles JLM420 and JLD505

[[

]]

Figure 2.9-2 EOC17 Nodal Powers for Bundles JLM420 and JLD505

[[

]]

Figure 2.9-3 EOC17 Nodal Void Fractions for Bundles JLM420 and JLD505

3.2 MEASUREMENT DETAILS

For the once-burnt bundle JLM420, measurements at 11 axial elevations for [[ ]] different fuel rods were made. Multiple measurements were made on the "reference" rod and on the "weak" rod. A total of [[ ]] separate rod measurements were made. For the reference rod, including four measurements for potential azimuthal dependencies in the measurements, a total of [[ ]] rod measurements were made. There were also [[ ]] measurements of the weak rod. [[ ]]

For the twice-burnt bundle JLD505, again measurements at 11 axial elevations for [[ ]] different fuel rods were planned, for a total of [[ ]] separate rod measurements had been made on [[ ]] rods. By the end of the campaign, [[ ]] rod measurements had been made because of the need to repeat measurements that had larger experimental counting uncertainties.

The first [[ ]] measurements were made with identical conditions to JLM420; with the exception of, new calibrations used with a new detector. After the first [[ ]] measurements, experimental difficulties were compensated for with a slight reconfiguration of the scanner while maintaining reference rod repeat measurements.

[[

]].

Figure 3.2-1 provides a graphical description of the measurement heights with respect to spacers and rod lengths.

[[

]]

Figure 3.2-1 Locations of Spacers and Axial Measurement Points

Table 5.2-1

Results for Adapted Off-line – Bundle JLM420

Height from BAZ (in.)	Std Dev {(P11/Meas)-1} (Comparison Std Dev)	Std Dev of [[ ]] Measurements of Rod [[ ]] (Measurement Reproducibility)	Corrected Std Dev
[[			
			]]

Table 5.2-2

Results for Non-Adapted Off-line – Bundle JLM420

Height from BAZ (in.)	Std Dev {(P11/Meas)-1} (Comparison Std Dev)	Std Dev of [[ ]] Measurements of Rod [[ ]] (Measurement Reproducibility)	Corrected Std Dev
[[			
			]]

Table 5.3-1

Results for Adapted Off-line – Bundle JLD505

Height from BAZ (in.)	Std Dev {(P11/Meas)-1} (Comparison Std Dev)	Std Dev of [[ ]] Measurements of Rod [[ ]] (Measurement Reproducibility)	Corrected Std Dev
[[			
			]]

Table 5.3-2

Results for Non-Adapted Off-line – Bundle JLD505

Height from BAZ (in.)	Std Dev {(P11/Meas)-1} (Comparison Std Dev)	Std Dev of [[ ]] Measurements of Rod [[ ]] (Measurement Reproducibility)	Corrected Std Dev
[[			
			]]

[[

]]

Figure 5.4.1-2. Measured Normalized ^{140}La for Bundle JLM420 (93 in. to 123 in.)

[[

]]

Figure 5.4.1-6. Pin-by-Pin {(TGBLA/Meas)-1} For Bundle JLM420 (93 in. to 123 in.)

[[

]]

Figure 5.4.2-4. TGBLA Predicted Normalized ^{140}La for Bundle JLD505 (93 in. to 123 in.)

[[

]]

Figure 5.4.2-5. TGBLA Predicted Normalized ^{140}La for Bundle JLD505 (27 in. to 87 in.)

[[

]]

Figure 5.4.2-6. Pin-by-Pin {(TGBLA/Meas)-1} For Bundle JLD505 (93 in. to 123 in.)

[[

]]

Figure 5.4.2-7. Pin-by-Pin {(TGBLA/Meas)-1} For Bundle JLD505 (27 in. to 87 in.)

6. PIN NODAL, BUNDLE, AND AXIAL ROOT MEAN SQUARE (RMS) COMPARISONS

The traditional comparison process provides insights as to the comparison of pin-by-pin power distribution within an X-Y plane, but the axial shape of the comparison is eliminated from consideration by the normalization process. This section provides a different view of the comparison process, analogous to the techniques common to the TIP comparison process. Similar to the TIP comparison process, the following three quantities are evaluated and compared:

- Pin Nodal RMS
- Rod RMS
- Axial Average RMS

In these comparisons, all measurements at all elevations are normalized to a value of 1.0. The Pin Nodal RMS evaluations provide insights as to the ability of the code packages to calculate the fuel rod kW/ft for a particular height of a particular fuel rod. The Rod RMS evaluations provide insights as to the ability of the code package to calculate the axially integrated fuel rod power. The axial average RMS evaluation provides insights as to the accuracy with which the bundle average axial power distribution is calculated. As contrasted with the TIP comparison process (See Appendix A), however, where all TIP strings have the same number of measurements, it is noted that not all rods that are gamma scanned in the fuel assembly are measured for ^{140}La, and the number of measurements finally obtained for each rod j may be different. For example, for part length rods there will be fewer measurements than for full-length rods. Also, for various reasons, there may not be measurements finally available for all axial elevations of all rods. Some data at a particular elevation may be missing, or the experimental counting uncertainties may be too large, causing the data for this measurement to be eliminated. Also, there may be multiple measurements for any particular rod. For the purpose of the statistical comparisons, the average value of all measurements for any particular axial elevation of each rod is computed, and the average value of these measurements at that location are used. The following table provides more details. The first set is for the TGBLA comparisons, while the second is for the PANAC11 based comparisons.

Height from BAZ	JLD505	JLM420		Height from BAZ	JLD505	JLM420
27	42	58		27	42	58
45	54	58		45	54	58
63	54	58		63	54	58
81	54	58		81	54	58
87	46	49		87	46	49
93	46	49		90	46	49
99	46	49		93	46	49
111	46	49		99	46	49
123	46	49		102	46	49
Total	434	477		111	46	49
				123	46	49
				Total	526	575

Table 6.0-1 Number of Measurements

Description of Statistics

6.1.1 Definitions

Let:

M(k, j) = Normalized Measured ^{140}La at axial elevation k for rod j

C(k, j) = Normalized Calculated (predicted) ^{140}Ba at axial elevation k for rod j

K(j) = Number of axial measurements for rod j

J = Number of rods for which measurements are available for this fuel assembly

J(k) = Number of measurements made at each axial level k

N = Total number of measurements (all rods at all elevations)

The measured ^{140}La and calculated ^{140}Ba are normalized in the same manner, as follows:

[[

]]

6.1.2 Pin Nodal RMS

[[ ]]

6.1.3 Rod RMS

The axially integrated rod power for those axial points where measurements are made is first calculated. There can be a different number of points for each different rod.

[[ ]]

6.1.4 Axial Average RMS

First, the average value at each axial level is calculated for all measured points ($\bar{M}_k$) and for all calculated points ($\bar{C}_k$). These average values are then normalized to an average value of 1.0. At each axial level, the RMS of the difference between the $\bar{M}_k$ and $\bar{C}_k$ is computed.

[[ ]]

6.2 PIN NODAL, ROD AVERAGED, AND AXIAL AVERAGE STATISTICAL SUMMARY

The pin nodal, rod averaged, and axial average statistics for each of the three analytical comparisons for the two bundles gamma scanned at FitzPatrick are provided below. As will be seen later, the TIP comparisons (Off-line non-adapted calculated TIPS compared to measured TIPs) will document a cycle average of [[ ]] nodal RMS value (with [[ ]] for the end of cycle TIP comparison). This TIP value represents (more or less) a result averaged over the four bundles surrounding the TIP string. This compares to the gamma scan values of between [[ ]] for the pin nodal RMS.

Thus the pin nodal gamma scan results are of the same order of magnitude of the TIP comparisons, and the gamma scan and the TIP results are consistent and complement each other. Note that the statistics presented in the following three tables are for each bundle separately.

- Table 6.2-1. Pin Nodal, Rod Averaged, and Axial Average Statistical Summary Adapted Off-line
- Table 6.2-2. Pin Nodal, Rod Averaged, and Axial Average Statistical Summary Off-line
- Table 6.2-3. Pin Nodal, Rod Averaged, and Axial Average Statistical Summary Nodal Depletions

Table 6.2-1.

Pin Nodal, Rod Averaged, and Axial Average Statistical Summary – Adapted Off-line

Bundle	Pin Nodal RMS	Rod Averaged RMS	Axial Averaged RMS
JLM420	[[		
JLD505			]]

Table 6.2-2.

Pin Nodal, Rod Averaged, and Axial Average Statistical Summary Off-line

Bundle	Pin Nodal RMS	Rod Averaged RMS	Axial Averaged RMS
JLM420	[[		
JLD505			]]

Table 6.2-3.

Pin Nodal, Rod Averaged, and Axial Average Statistical Summary – Nodal Depletions

Bundle	Pin Nodal RMS	Rod Averaged RMS	Axial Averaged RMS
JLM420	[[		
JLD505			]]

6.3 SUMMARY PLOTS OF PIN NODAL RMS

6.3.1 Summary Plot for Adapted Off-line – Pin Nodal RMS

This section provides a comparison of the normal on-line TIP and LPRM-adapted design tools with the results of the gamma scan. This case is generated with TIP and LPRM shape adapted PANAC11 core tracking. This adapted off-line core tracking reproduces the thermal limits seen in the on-line monitoring. Figure 6.3.1-1. combines the results of the prediction of ^{140}Ba generated with PANAC11 for both measured bundles versus the measured ^{140}La.

The RMS value for this comparison is [[ ]]. This value represents the combined RMS value for both bundles. In Figure 6.3.1-1., the predicted ^{140}Ba is the normalized predicted ^{140}Ba number density from TGBLA06 for that particular rod, and the measured ^{140}La is the normalized measured decay corrected count rates for ^{140}La. Both predicted and measured values are normalized to an average value of 1.0.

[[

]]

Figure 6.3.1-1. Combined Pin Nodal RMS for Bundles JLM420 and JLD505 for Adapted Off-line

6.3.2 Summary Plot for Off-line – Pin Nodal RMS

This comparison provides a summary of the off-line non-adapted results with the gamma scan measurements. Figure 6.3.2-1 combines the results of the prediction of ^{140}Ba generated for both measured bundles versus the measured ^{140}La.

The RMS value for this comparison is [[ ]]. This value represents the combined RMS value for both bundles. [[ ]]. Again, both predicted and measured values are normalized to an average value of 1.0.

[[

]]

Figure 6.3.2-1. Combined Pin Nodal RMS for Bundles JLM420 and JLD505 for Off-line

6.3.3 Summary Plot for Nodal Depletions – Pin Nodal RMS

This case provides a comparison of the use of the lattice code TGBLA06 to compute the predicted ^{140}Ba (generated by replicating the nodal tracking from the PANAC11 off-line core tracking with the lattice code) with the gamma scan measurements. In this approach the nodal PANAC11 values for power density, void fraction, and control rod presence are used in the TGBLA06 code to deplete to the end of cycle. Figure 6.3.3-1. combines the results of the prediction of ^{140}Ba generated with TGBLA06 for both measured bundles versus the measured ^{140}La.

The RMS value for this comparison is [[ ]]. This value represents the combined RMS value for both bundles.

[[

]]

Figure 6.3.3-1. Combined Pin Nodal RMS for Bundles JLM420 and JLD505 for Nodal Depletions

6.4 SUMMARY OF ROD AVERAGED RMS COMPARISONS

6.4.1 Rod Averaged RMS Comparisons for Adapted Off-line

Figures 6.4.1-1. and 6.4.1-2. compare the measured ^{140}La and predicted ^{140}Ba distributions on a rod-by-rod basis for the t o gamma scanned bundles. In these figures, the "radial" value is derived by first calculating the "average" value of the (normalized to 1.0 over all measurements) ^{140}La measured for that fuel rod. The average value of ^{140}Ba predicted for that same number of axial elevations is then computed. Corner rods (tan), rods next to corner rods (grey), water rods (yellow), and gadolinium rods (green) are color coded in the lattice map. For bundle JLM420, the rod average RMS value is [[ ]]. For bundle JLD505, the rod average RMS value is [[ ]].

[[

]]

Figure 6.4.1-1. Rod Averaged RMS for Bundle JLM420 Adapted Off-line

[[

]]

Figure 6.4.1-2. Rod Averaged RMS for Bundle JLD505 Adapted Off-line

6.4.2 Rod Averaged RMS Comparisons for Off-line

Figures 6.4.2-1. and 6.4.2-2. compare the measured ^{140}La and predicted ^{140}Ba distributions on a rod-by-rod basis for the two gamma scanned bundles for the Off-line core tracking process. Corner rods (tan), rods next to corner rods (grey), water rods (yellow), and gadolinium rods (green) are color coded in the lattice map. For bundle JLM420 the rod average RMS value is [[ ]]. For bundle JLD505 the rod average RMS value is [[ ]].

[[

]]

Figure 6.4.2-1. Rod Averaged RMS for Bundle JLM420 Off-line

[[

]]

Figure 6.4.2-2. Rod Averaged RMS for Bundle JLD505 Off-line

6.4.3 Rod Averaged RMS Comparisons for Nodal Depletions

Figures 6.4.3-1. and 6.4.3-2. compare the measured ^{140}La and predicted ^{140}Ba distributions on a rod-by-rod basis for the two gamma scanned bundles for the TGBLA nodal depletion process. Corner rods (tan), rods next to corner rods (grey), water rods (yellow), and gadolinium rods (green) are color coded in the lattice map. For bundle JLM420, the rod average RMS value is [[ ]]. For bundle JLD505, the rod average RMS value is [[ ]].

[[

]]

Figure 6.4.3-1. Rod Averaged RMS for Bundle JLM420 Nodal Depletion

[[

]]

Figure 6.4.3-2. Rod Averaged RMS for Bundle JLD505 Nodal Depletion

6.5 SUMMARY OF AXIAL AVERAGED RMS COMPARISONS

6.5.1 Axial Averaged RMS Comparisons for Adapted Off-line

Figures 6.5.1-1. and 6.5.1-2. compare the axial averaged predicted ^{140}Ba and the measured ^{140}La for the TIP and LPRM adapted case. For bundle JLM420, the axial RMS value is [[ ]]. For bundle JLD505, the axial RMS value is [[ ]].

[[

]]

Figure 6.5.1-1. Axial Averaged Predicted Ba and Measured La for Bundle JLM420 Adapted Off-line

[[

]]

Figure 6.5.1-2. Axial Averaged Predicted Ba and Measured La for Bundle JLD505 Adapted Off-line

6.5.2 Axial Averaged RMS Comparisons for Off-line

Figures 6.5.2-1. and 6.5.2-2. compare the axial averaged predicted ^{140}Ba and the measured ^{140}La for the off-line case (i.e., non-adapted off-line core tracking). For bundle JLM420, the axial RMS value is [[ ]]. For bundle JLD505, the axial RMS value is [[ ]].

[[

]]

Figure 6.5.2-1. Axial Averaged Predicted Ba and Measured La for Bundle JLM420 Off-line

[[

]]

Figure 6.5.2-2. Axial Averaged Predicted Ba and Measured La for Bundle JLD505 Off-line

7.2 SUMMARY OF MEASURED UNCERTAINTIES –PIN-BY-PIN XY

As documented in Sections 5.2 and 5.3, the results of the gamma scan comparisons for all three modeling approaches provide better statistics (using the traditional basis approach) than the uncertainties summarized in NEDC-32601P-A.

This set of comparisons is based on normalization of the data to 1.0 for each axial level separately. In these comparisons, therefore, the effects of bundle axial and radial power distributions have been removed. These are lattice comparisons, or XY comparisons, consistent with the traditional approach as summarized in Section 5.2. As such, the measured and predicted pin values at each axial level are normalized to 1.0 for that level. The value reported for the Corrected Standard Deviation is therefore the average of the standard deviations for all levels (i.e., the average is not weighted by the number of pins measured at each level).

The measured comparison values explicitly include the actual effects of all [[

]]

Table 7.2-1

Comparisons of Pin Power Peaking Measurement Statistics

Bundle	Core Tracking Modeling	Corrected Std Dev
JLM420	Adapted Off-line	[[
JLM420	Off-Line	
JLM420	Nodal Depletion	
JLD505	Adapted Off-line	
JLD505	Off-Line	
JLD505	Nodal Depletion	]]

As shown in Table 7.2-1, the largest uncertainty is [[ ]], which is significantly smaller than the value of [[ ]] from Section 3.1.4 of NEDC-32601P-A.

[[

]]

Figure 8.2-1. {(TGBLA/Meas)-1} For Bundle JLM420 at 27 In.

[[

]]

Figure 8.2-2. {(TGBLA/Meas)-1} For Bundle JLM420 at 45 In.

[[

]]

Figure 8.2-3. {(TGBLA/Meas)-1} For Bundle JLM420 at 63 In.

[[

]]

Figure 8.2-4. {(TGBLA/Meas)-1} For Bundle JLM420 at 81 In.

[[

]]

Figure 8.2-5. {(TGBLA/Meas)-1} For Bundle JLM420 at 87 In.

[[

]]

Figure 8.2-6. {(TGBLA/Meas)-1} For Bundle JLM420 at 93 In.

[[

]]

Figure 8.2-7. {(TGBLA/Meas)-1} For Bundle JLM420 at 99 In.

[[

]]

Figure 8.2-8. {(TGBLA/Meas)-1} For Bundle JLM420 at 111 In.

[[

]]

Figure 8.2-9. {(TGBLA/Meas)-1} For Bundle JLM420 at 123 In.

8.3 XYZ PLOTS OF {(P11/MEAS)-1} PIN-BY-PIN ERRORS – BUNDLE JLM420 – OFF-LINE ADAPTATION

In Figures 8.3-1. through 8.3-9., the quantity {(P11/Measured)-1} is displayed for each pin at the eleven elevations for which PANAC11 predicted pin-by-pin ^{140}Ba was compared to the measured ^{140} La data. In these figures, the lattice is viewed from the location of the instrument tube again, the narrow-narrow corner is nearest the front, and the control rod location would be towards the back of the figure.

[[

]].

[[

]]

Figure 8.3-1. {(P11/Meas)-1} For Bundle JLM420 at 27 In.

[[

]]

Figure 8.3-2. {(P11/Meas)-1} For Bundle JLM420 at 45 In.

[[

]]

Figure 8.3-3. {(P11/Meas)-1} For Bundle JLM420 at 63 In.

[[

]]

Figure 8.3-4. {(P11/Meas)-1} For Bundle JLM420 at 81 In.

[[

]]

Figure 8.3-5. {(P11/Meas)-1} For Bundle JLM420 at 87 In.

[[

]]

Figure 8.3-6. {(P11/Meas)-1} For Bundle JLM420 at 90 In.

[[

]]

Figure 8.3-7. {(P11/Meas)-1} For Bundle JLM420 at 93 In.

[[

]]

Figure 8.3-8. {(P11/Meas)-1} For Bundle JLM420 at 99 In.

[[

]]

Figure 8.3-9. {(P11/Meas)-1} For Bundle JLM420 at 102 In.

[[

]]

Figure 8.3-10. {(P11/Meas)-1} For Bundle JLM420 at 111 In.

[[

]]

Figure 8.3-11. {(P11/Meas)-1} For Bundle JLM420 at 123 In.

8.4 XYZ PLOTS OF {(TGBLA/MEAS)-1} PIN-BY-PIN ERRORS – BUNDLE JLD505

In Figures 8.4-1. through 8.4-9., the quantity {(TGBLA/Measured)-1} is displayed for bundle JLD5050 for each pin at the nine elevations for which TGBLA06 nodal depletions were compared to the measured data. In these figures, the lattice is viewed from the location of the instrument tube that is, the narrow-narrow corner is nearest the front, and the control rod location would be towards the back of the figure. Each row of fuel pins is assigned a different color in these plots.

[[

]]

[[

]]

Figure 8.4-1. {(TGBLA/Meas)-1} For Bundle JLD505 at 27 In.

[[

]]

Figure 8.4-2. {(TGBLA/Meas)-1} For Bundle JLD505 at 45 In.

[[

]]

Figure 8.4-3. {(TGBLA/Meas)-1} For Bundle JLD505 at 63 In.

[[

]]

Figure 8.4-4. {(TGBLA/Meas)-1} For Bundle JLD505 at 81 In.

[[

]]

Figure 8.4-5. {(TGBLA/Meas)-1} For Bundle JLD505 at 87 In.

[[

]]

Figure 8.4-6. {(TGBLA/Meas)-1} For Bundle JLD505 at 93 In.

[[

]]

Figure 8.4-7. {(TGBLA/Meas)-1} For Bundle JLD505 at 99 In.

[[

]]

Figure 8.4-8. {(TGBLA/Meas)-1} For Bundle JLD505 at 111 In.

[[

]]

Figure 8.4-9. {(TGBLA/Meas)-1} For Bundle JLD505 at 123 In.

8.5 XYZ PLOTS OF {(P11/MEAS)-1} PIN-BY-PIN ERRORS – BUNDLE JLD505 – OFF-LINE ADAPTATION

In Figures 8.5-1. through 8.5-9., the quantity {(P11/Measured)-1} is displayed for each pin at the eleven elevations for which PANAC11 predicted pin-by-pin ^{140}Ba was compared to the measured ^{140} La data. In these figures, the lattice is viewed from the location of the instrument tube again, the narrow-narrow corner is nearest the front, and the control rod location would be towards the back of the figure.

[[

]].

[[

]]

Figure 8.5-1. {(P11/Meas)-1} For Bundle JLD505 at 27 In.

[[

]]

Figure 8.5-2. {(P11/Meas)-1} For Bundle JLD505 at 45 In.

[[

]]

Figure 8.5-3. {(P11/Meas)-1} For Bundle JLD505 at 63 In.

[[

]]

Figure 8.5-4. {(P11/Meas)-1} For Bundle JLD505 at 81 In.

[[

]]

Figure 8.5-5. {(P11/Meas)-1} For Bundle JLD505 at 87 In.

[[

]]

Figure 8.5-6. {(P11/Meas)-1} For Bundle JLD505 at 90 In.

[[

]]

Figure 8.5-7. {(P11/Meas)-1} For Bundle JLD505 at 93 In.

[[

]]

Figure 8.5-8. {(P11/Meas)-1} For Bundle JLD505 at 99 In.

[[

]]

Figure 8.5-9. {(P11/Meas)-1} For Bundle JLD505 at 102 In.

[[

]]

Figure 8.5-10. {(P11/Meas)-1} For Bundle JLD505 at 111 In.

[[

]]

Figure 8.5-11. {(P11/Meas)-1} For Bundle JLD505 at 123 In.

8.6 POTENTIAL TRENDS [[

]]

[[

]]

[[

]]

Figure 8.6-1. {(P11/Meas)-1} vs. [[ ]]

[[

]]

Figure 8.6-2. {(P11/Meas)-1} vs. [[ ]]

[[

]]

Figure 8.6-3. {(P11/Meas)-1} vs. [[ ]]

[[

]]

Figure 8.6-4. {(P11/Meas)-1} vs. [[ ]]

8.6.1 Potential Impact [[ ]]

[[

]]

9. REFERENCES

1. Letter from USNRC to G. A. Watford (GE), "Amendment 26 to GE Licensing Topical Report NEDE-24011-P-A, 'GESTAR II' - Implementing Improved GE Steady-State Methods," November 10, 1999.
2. GE Nuclear Energy, "Power Distribution Uncertainties for Safety Limit MCPR Evaluations," NEDC-32694P-A, August 1999.
3. GE Nuclear Energy, "Advanced Methods Power Distribution Uncertainties for Core Monitoring," NEDC-32773P, Revision 1, January 1999.
4. GE Hitachi Nuclear Energy, NEDC-33173P, Supplement 2 Part 1, Licensing Topical Report, Applicability of GE Methods to Expanded Operating Domains Power Distribution Validation for Cofrentes Cycle 13, August 2009.
5. GE Nuclear Energy, "Methodology and Uncertainties for Safety Limit MCPR Evaluations," NEDC-32601P-A, August 1999.
6. GE Nuclear Energy, Letter, J. S. Post to NRC, Document Control Desk, "Part 21 Evaluation; Power Distribution Uncertainty Reassessment," MFN05-082, August 18, 2005.
7. GE Nuclear Energy "Applicability of GE Methods to Expanded Operating Domains" NEDC-33173P," February 2006.
8. Letter from TB Blount (NRC) to JG Head (GEH), Subject: Final Safety Evaluation for GE Hitachi Nuclear Energy Americas, LLC Licensing Topical Report NEDC-33173P, "Applicability of GE Methods To Expanded Operating Domains" (TAC No. MD0277 , July 21, 2009.

Appendix A OFF-LINE NON-ADAPTED TIP COMPARISONS

The definitions of statistics used in these TIP comparisons are provided in the Cofrentes LTR.

A.1 CYCLE 17 NON-ADAPTED TIP SETS

There were only eight TIP sets run during the cycle. These are summarized in Table A.1-1 and Figure A.1-1.

From sometime after April, 2006 until very near the end of cycle in October, 2006, there was apparently a problem with one of the TIP machines. Apparently for these TIPs, the values were not normalized to the same integral value as the TIP data from the other TIP machines. As a result, the nodal RMS difference between the measured and calculated TIPs increased dramatically for the June, 2006 TIP set, as shown in the following table and plots. This problem was apparently corrected by the last TIP set.

However, this did not affect the 3DM / PANAC11 shape adaptive process, in that the radial component of the TIP data is not used in the adaptive process. Therefore the plant thermal margins calculated in the shape adaptive process were not affected, as the axial shape of the TIP measurements was not affected by the TIP mechanical problems, nor was the LPRM calibration process in 3DM / PANAC11. In addition, the exposure and void history accumulation in the on-line 3DM / PANAC11 is based on the non-adapted power distribution. Thus, the only implication is that the TIP radial RMS for this one case is seen to be quite large, with no actual impact on plant monitoring due to the inherent robustness of the 3DM / PANAC11 system.

A.2 CYCLE 17 - COMPARISON OF CORE AVERAGE AXIAL TIPS – NON-ADAPTED

This subsection provides snapshots of the comparison of the measured and calculated core average axial TIPs at the eight exposure points in Cycle 17. The progression from a more bottom peaked power distribution at the middle of cycle to a more top peaked power distribution at the end of cycle can be inferred from the core average axial TIP plots.

Appendix B

L. M. Shiraishi, Gamma Scan Measurements of the Lead Test Assembly at The Duane Arnold Energy Center Following Cycle 8, NEDC-31569-P, April 1988

Appendix B is an archive document that was not prepared for US NRC submittal. It is Proprietary in its entirety and no Non-Proprietary version is provided.